The diazepam binding inhibitor's modulation of the GABA-A receptor is subunit-dependent

Jennifer S. Borchardt[1], Lucas M. Blecker[2], Kenneth A. Satyshur[2], and Cynthia Czajkowski[2]*

[1] Cellular and Molecular Biology Graduate Program, University of Wisconsin-Madison, Madison, WI, United States of America

[2]Department of Neuroscience, University of Wisconsin-Madison, Madison, WI, United States of America

* Corresponding author

Email: cmczajko@wisc.edu

Abstract

First synthesized in the 1950s, benzodiazepines are widely prescribed drugs that exert their anxiolytic, sedative and anticonvulsant actions by binding to GABA-A receptors, the main inhibitory ligand-gated ion channel in the brain. Scientists have long theorized that there exists an endogenous benzodiazepine, or endozepine, in the brain. While there is indirect evidence suggesting a peptide, the diazepam binding inhibitor, is capable of modulating the GABA-A receptor, direct evidence of the modulatory effects of the diazepam binding inhibitor is limited.

Here we take a reductionist approach to understand how purified diazepam binding inhibitor interacts with and affects GABA-A receptor activity. We used two-electrode voltage clamp electrophysiology to study how the effects of diazepam binding inhibitor vary with GABA-A receptor subunit composition, and found that GABA-evoked currents from α3-containing GABA-A receptors are weakly inhibited by the diazepam binding inhibitor, while currents from α5-containing receptors are positively modulated. We also used *in silico* protein-protein docking to visualize potential diazepam binding inhibitor/GABA-A receptor interactions that revealed diazepam binding inhibitor bound at the benzodiazepine α/γ binding site interface, which provides a structural framework for understanding diazepam binding inhibitor effects on GABA-A receptors. Our results provide novel insights into mechanisms underlying how the diazepam binding inhibitor modulates GABA-mediated inhibition in the brain.

Introduction

Since their discovery over fifty-five years ago, benzodiazepines (BZDs) have been some of the most widely prescribed drugs in the world, and have remained on the World Health Organization's list of essential drugs since the list's inception in 1977 [1]. BZDs are used to treat a variety of conditions, ranging from epilepsy to insomnia to anxiety [2-4], and mediate their

effects by binding to the main inhibitory neurotransmitter receptor in the brain, the gamma-aminobutyric acid-A receptor (GABAR) [5]. BZDs modulate GABAR activity, and thus alter neuronal signaling.

GABARs are heteropentamers comprised from nineteen possible subunits (α1-6, β1-3, γ1-3, δ, ε, θ, π and ρ1-3) that are expressed in distinct brain regions, with distinct pharmacological properties. There are two GABA binding sites in the extracellular interfaces between β and α subunits, while BZDs bind in an extracellular pocket at the α/γ subunit interface. BZDs, such as diazepam or flurazepam (FZM), can act as positive allosteric modulators (PAMs), which increase GABA-mediated currents, or negative allosteric modulators (NAMs) like methyl-6,7-dimethoxy-4-ethyl-beta-carboline-3-carboxylate (DMCM) which decrease GABA-elicited currents. Zero-modulators, such as flumazenil (FLZ, Ro15-1788), occupy the BZD site but do not alter GABA-elicited currents. The effects of some BZDs like Ro15-4513 depend on GABAR subunit composition. Ro15-4513 acts as PAM when interacting with $\alpha_4\beta_2\gamma_2$ and $\alpha_6\beta_2\gamma_2$ GABARs, but is a NAM when bound to $\alpha_1\beta_2\gamma_2$ receptors[6].

The presence a binding site on the GABAR for synthetically manufactured BZDs has long suggested the existence of an endogenous synthesized molecule that binds to the same site. In 1983, a candidate peptide was isolated from rat brain homogenates, which displaced tritiated diazepam in a radioligand binding assay [7]. This 10kD, 87 amino-acid protein was named the diazepam binding inhibitor (DBI). Recent DBI knock-down and over-expression studies in the thalamic reticular nucleus demonstrate that DBI works *in vivo* as a PAM where it potentiates GABA-mediated currents and suppresses epileptic activity[8]. In contrast, DBI knock-down in the subventricular zone of the lateral ventricles and in the hippocampal subgranular zone demonstrate that DBI and one of its peptide fragments, ODN, inhibit GABA-induced currents [9, 10], indicating that in these brain regions DBI and ODN work as NAMs of

68 GABARs. We hypothesized that the differences in DBI's modulatory effects are due to regional
69 differences in GABAR subunit expression and GABAR subunit composition.
70 Here, we used two-electrode voltage clamping and measured DBI effects on GABA-
71 activated currents from GABARs expressed in *Xenopus laevis* oocytes. Given DBI is highly
72 expressed in the hippocampus and thalamus [11, 12], we focused on $\alpha_5\beta_3\gamma_{2L}$ and $\alpha_3\beta_3\gamma_{2L}$
73 GABAR subtypes which are enriched in these regions [13]. We found that DBI positively
74 modulates $\alpha_5\beta_3\gamma_{2L}$ receptors, whereas DBI is a weak negative modulator of $\alpha_3\beta_3\gamma_{2L}$ GABARs. We
75 used *in silico* protein-protein docking to visualize potential DBI-GABAR interactions.

76 Materials and Methods

77 DBI expression and purification for functional testing

78 We used cDNA for human DBI isoform3 (GeneBank ID CAG33237.1) with a C-terminal
79 histidine tag in a pET28a vector. The plasmid was chemically transformed into BL21 DE3
80 competent cells, plated on LB-Kanamycin (Kan) agar plates, and grown overnight at 37°C. A
81 single colony was picked and grown overnight in a 5mL culture of LB with 250µg Kan while
82 shaking at 37°C. This culture was used to inoculate 500mL LB + Kan and the culture was grown
83 until OD_{600} reached 0.6-0.8. Protein expression was induced with IPTG (500µM) for 4 hours at
84 37°C. After induction, cells were pelleted by spinning at 10,000xg for 10min at 4°C. The
85 bacterial cell pellet was frozen at -80°C. Cell pellet was thawed and resuspended in 50mL
86 Buffer A (sodium phosphate, 50mM, pH 7.4; NaCl, 300mM) and 25mM imidazole (IDA) with a
87 protease inhibitor cocktail (pepstatin, aprotinin, leupeptin). After lysis using an Emulsiflex (ATA
88 Scientific, Taren Point, NSW Australia), samples were spun at 16800xg for 20min, 4°C. The
89 supernatant was bound to an Ni-NTA column which was pre-equilibrated in column buffer
90 (Buffer A and 10mM imidazole, pH 7.4). His-tagged DBI was eluted using elution buffer (Buffer
91 A and 250mM imidazole). A PD10 desalting column was used to remove imidazole, DBI was
92 eluted in Buffer A. DBI molecular weight was verified via 15% SDS-PAGE stained with

93 Coomasie blue and protein level quantified using a Nanodrop 2000 (Thermo Fisher Scientific,
94 Waltham, MA), using an absorption coefficient of 1.68. DBI with the histidine tag attached has a
95 mass of 10.87kDa. All data shown used purified His-tagged DBI, whose effects were similar to
96 untagged DBI (data not shown).

97 DBI purification for NMR

98 DBI was transformed into BL21 DE3 cells, grown in ^{15}N-labeled M9 media, and purified
99 as described above. A ^{1}H-^{15}N HSQC spectrum was obtained using a Bruker Avance III 600 MHz
100 spectrometer, with 5-10% D_2O added to the protein sample. The spectrum was collected at
101 25°C. Data were processed using NMRPipe [14] and analyzed using CcpNmr analysis [15].

102 Expression in *Xenopus laevis* oocytes

103 Rat cDNA encoding the GABAR α3, α5, β3 and γ2L subunits subcloned into the pUNIV
104 vector [16] were used. cRNA was transcribed from NotI-digested cDNA using the mMessage T7
105 kit (Ambion, Austin, TX). *Xenopus laevis* oocytes were harvested and prepared as described
106 previously [17]. Oocytes were injected with 27-54nL of GABAR subunit cRNA at 10ng/μL α,
107 10ng/μL β and 100ng/μL γ2L following previously described methods [18], stored at 16°C in
108 ND96 buffer (96mM NaCl, 2mM KCl, 1mM MgCl2, 1.8mM CaCl2, and 5mM HEPES, pH 7.2)
109 supplemented with 100μg/ml bovine serum albumin and gentamycin and recorded from 2-7
110 days after injection.

111 Two electrode voltage clamp

112 Electrophysiological recordings were performed as described previously [19]. Oocytes
113 expressing GABARs were held at -40 to -80 mV under a two-electrode voltage clamp and
114 continuously perfused with ND96 at 5mL/min in a 200 μL volume chamber. Boroscilicate glass
115 electrodes (0.4-1.0mΩ, Warner Instruments, Hamden, CT) were filled with 3M KCl. Data were
116 collected at room temperature using two different volatage clamps. One was a GeneClamp 500

117 (Molecular Devices, Sunnyvale, CA) interfaced to a computer via a Digidata 1200 device
118 (Molecular Devices) with data recorded using Whole Cell Program, version 3.6.7 (J. Dempster,
119 University of Strathclyde, Glasgow, UK). The other was an Oocyte Clamp OC-725A (Warner
120 Instruments) with a Digidata 1440A (Molecular Devices) with data recorded using AxoScope,
121 pCLAMP 10 (Molecular Devices). Data and results obtained from the clamps were
122 indistinguishable.

123 A stock solution of 1 M GABA (Sigma-Aldrich, St Louis, MO) was made in water, stored
124 at -20°C and thawed before use. GABA dilutions for experiments were prepared fresh daily in
125 ND96. A stock solution of 10 mM FZM (Sigma/RBI, Natick, MA) in water was diluted in ND96 for
126 working concentrations daily. A stock solution of 10mM DMCM (Sigma/RBI, Natick, MA) was
127 prepared in dimethyl sulfoxide and diluted daily in ND96 for working concentrations in which the
128 final concentration of dimethyl sulfoxide (≤0.1%) did not affect GABAR function.

129 Concentration-response analysis

130 GABA concentration-response curves were determined as described previously [19].
131 Seven concentrations of GABA (1μM, 3μM, 10μM, 30μM, 100μM, 1mM and 10mM) were used
132 to determine GABA EC50 values. Concentration-response data were fit using Prism version 8.4
133 (GraphPad Software Inc., San Diego, CA) to the equation: I = Imax/[1 + (EC50/[A]nH)], in which
134 I is the peak current response to a given GABA concentration, Imax is the maximal amplitude of
135 GABA activated current, EC50 is the GABA concentration that produces the half-maximal
136 response, [A] is test GABA concentration, and nH is the Hill coefficient.

137 Drug modulation

138 Drug modulation was measured at GABA EC_{20} and evaluated as $I_{GABA+Drug}/I_{GABA}$, where
139 $I_{GABA+Drug}$ is the GABA-mediated current in the presence of drug and I_{GABA} is the GABA-mediated
140 current in the absence of drug. To measure drug modulation, a brief 5 sec application of GABA
141 EC_{20} was applied and followed immediately by a 5 sec application of GABA EC_{20}+Drug. When

142 multiple drugs were applied to a single oocyte, GABA EC_{20} was applied following drug treatment
143 until current amplitudes returned to initial GABA EC_{20} level to ensure complete washout of drugs
144 between different drug treatments.

145 Protein-protein docking

146 We made $\alpha_3\beta_3\gamma_{2L}$ and $\alpha_5\beta_3\gamma_{2L}$ GABAR homology models based on the cryoEM structure
147 of the $\alpha_1\beta_3\gamma_{2L}$ GABAR obtained in the presence of the BZD alprazolam (PDB 6HUO) [20]. The
148 homology models were built on Sybyl (Tripos Inc). The GABAR α3 or α5 sequences were
149 manually threaded on to the cryoEM model of the $\alpha_1\beta_3\gamma_{2L}$ GABAR based on their sequence
150 alignment with the α1 subunit using the graphical interface of the Sybyl program. After resolving
151 steric clashes, either manually or by using focused minimization, the resulting structures were
152 subject to whole molecule energy minimization using the Tripos force field. Gasteiger-Huckel
153 charges were added to the atoms, and the dielectric function set at 1.0. After Simplex initial
154 minimization, the Powell function in Tripos was used to minimize to a termination gradient of
155 0.05 kcal/(mol x angstrom). The GABAR model images were developed using PyMOL
156 (Schrödinger, LLC, New York). BZD alprazolam was removed from models prior to docking.

157 Protein-protein interactions between the $\alpha_3\beta_3\gamma_{2L}$ and $\alpha_5\beta_3\gamma_{2L}$ GABAR models and the
158 unliganded human DBI crystal structure (PDB 2FJ9) [21] were identified using ClusPro, a web-
159 based program for computational docking of proteins [22-24]. ClusPro analyzes 70,000 rotations
160 of the ligand and generates up to 30 highly populated clusters of ligand structures docked in
161 similar locations on the receptor with low energy scores. Clusters are ranked by population size
162 rather than an energy score. Docking clusters selected for analysis were based on their
163 proximity to the BZD binding site. We analyzed the hydrogen bonding between the GABAR
164 alpha subunits and DBI and the GABAR gamma subunit and DBI using Pymol's hydrogen
165 bonding feature.

166 ## Statistical analysis

167 All data were from at least three different oocytes from at least two different frogs. Data
168 are represented as mean ± SD. Significant differences in drug modulation between subunit
169 compositions were calculated via Kruskal-Wallis test with a Dunn's multiple comparisons (Prism
170 v8.4, GraphPad Software Inc, San Diego, CA). This test was selected due to the nonparametric
171 distribution of data. Statistical differences in GABA+drug versus GABA alone currents elicited
172 from the same oocyte were calculated using a paired t-test using Prism software.

173 The effects of DBI on $\alpha_5\beta_3\gamma_{2L}$ GABA-elicited currents were more variable than effects
174 observed with FZM, a BZD (coefficient of variation for FZM $\alpha_5\beta_3\gamma_{2L}$ is 17.2%, DBI is 36.0%). The
175 variation was not correlated with DBI purification batch nor oocyte/frog. We hypothesize that
176 flexibility and conformation dynamics of DBI (11kDa) may contribute to the increased variability
177 of its effects as compared to a small BZD drug.

178

179 # Results

180 In order to study the effects of DBI on the GABAR receptor, we needed milligram
181 quantities of pure, non-aggregated DBI folded predominantly in a single conformation. We used
182 a histidine-tagged human DBI construct (His-DBI) inserted into a pET28A vector, which is
183 optimized for inducible expression of protein in bacterial cells [25]. We expressed the His-DBI in
184 BL21 *E. coli* cells and purified the protein as described in Methods. DBI purity and and size was
185 evaluated using 15% SDS-PAGE (Fig 1A). Following purification, a single coomassie blue
186 stained band was observed with a molecular weight of 11kDa. DBI with the histidine tag
187 attached has a mass of 10.87kDa. Heteronuclear single quantum correlation (HSQC) nuclear
188 magnetic resonance (NMR) of ^{15}N-labeled DBI demonstrated that our DBI purification process
189 yielded pure, non-aggregated and folded protein in a single conformation, as the number of

190 peaks were very close to the total number of residues in the His-tagged DBI, spectral dispersion
191 was good, and the linewidths were relatively uniform (Fig 1B).
192
193 **Fig 1 - Purified DBI is non-aggregated and folded in a single conformation.** (A) 15% SDS-
194 PAGE showing coomassie blue stained molecular weight marker proteins at 25, 20, 15 and
195 10kDa, and purified histidine-tagged DBI running at its expected size 11kD. (B) ^{1}H-^{15}N HSQC
196 spectrum from DBI grown in ^{15}N M9 media shows close to expected number of peaks (93
197 expected, 96 detected), good spectral dispersion and low noise, indicating purified DBI is folded
198 and non-aggregated.
199
200 We expressed $\alpha_3\beta_3\gamma_{2L}$ and $\alpha_5\beta_3\gamma_{2L}$ GABARs in *Xenopus laevis* oocytes and used two-
201 electrode voltage-clamping to measure and compare the effects of a BZD PAM (FZM), a BZD
202 NAM (DMCM) and DBI on GABA-elicited currents. Initially, we measured GABA concentration
203 responses from oocytes expressing $\alpha_3\beta_3\gamma_{2L}$ and $\alpha_5\beta_3\gamma_{2L}$ GABARs. GABA EC_{50} values were
204 47±11.8 μM, n=5 for $\alpha_3\beta_3\gamma_{2L}$ GABARs (Fig 2A) and 34±8.6 μM, n=3 for $\alpha_5\beta_3\gamma_{2L}$ GABARs (Fig
205 2B), which are consistent with previously published results [26, 27].
206
207 **Fig 2 – GABA dose response curves for $\alpha_3\beta_3\gamma_{2L}$ and $\alpha_5\beta_3\gamma_{2L}$ GABARs**. Current responses
208 from oocytes expressing $\alpha_3\beta_3\gamma_{2L}$ (A) and $\alpha_5\beta_3\gamma_{2L}$ (B) GABARs were fit by non-linear regression
209 as described in Methods. Data were normalized to maximal GABA current obtained from curve
210 fits and averaged from three to five different oocytes, with error bars showing SD.
211
212 To evaluate and compare the effects of the positive BZD modulator, FZM, the negative
213 BZD modulator, DMCM and DBI, we applied a low GABA EC20 concentration and then co-
214 applied FZM (10μM), DMCM (10μM) or DBI (50μM) with GABA EC20 (Fig 3A). FZM (10μM)
215 significantly increased GABA currents from oocytes expressing $\alpha_3\beta_3\gamma_{2L}$ and $\alpha_5\beta_3\gamma_{2L}$ GABARs

216 2.7- and 2.1 fold, respectively (Fig. 3; paired t-test $p<0.0001$ for both GABAR subtypes). The
217 effects of FZM on α3-containing receptors compared to α5-containing receptors were not
218 significantly different (Fig 3B, Dunn's $p>0.999$). DMCM (10μM) significantly inhibited GABA
219 currents from both $\alpha_3\beta_3\gamma_{2L}$ and $\alpha_5\beta_3\gamma_{2L}$ GABARs (Fig 3) and the effects of DMCM on α3-
220 containing versus α5-containing GABARs were not significantly different (Fig 3B, Dunn's
221 $p>0.999$).
222
223 **Fig 3 – DBI modulates $\alpha_3\beta_3\gamma_{2L}$ differently than $\alpha_5\beta_3\gamma_{2L}$ GABARs**. (A) Sample current traces
224 from oocytes expressing $\alpha_3\beta_3\gamma_{2L}$ (top) and $\alpha_5\beta_3\gamma_{2L}$ (bottom) GABARs showing co-application of
225 FZM (10μM) with GABA EC20 increased GABA current and co-application of DMCM (10μM)
226 decreased current. DBI (50μM) slightly decreased currents from $\alpha_3\beta_3\gamma_{2L}$ GABARs and increased
227 currents from $\alpha_5\beta_3\gamma_{2L}$ GABARs. (B) Effects of FZM, DMCM and DBI are plotted as
228 $I_{Drug+GABA}/I_{GABA}$. Data from individual occytes are shown as filled circles, bar graphs represent
229 mean +/- SD. Dotted line at 1 represents no effect of drug. DBI effects on $\alpha_3\beta_3\gamma_{2L}$ and $\alpha_5\beta_3\gamma_{2L}$
230 GABARs are significantly different from each other, while the effects of FZM and DMCM are
231 similar for both GABAR subtypes (Kruskal-Wallis test). (C) Table displaying mean +/- SD of
232 FZM, DMCM and DBI effects on currents from $\alpha_3\beta_3\gamma_{2L}$ and $\alpha_5\beta_3\gamma_{2L}$ GABAR, n = number of
233 oocytes. Currents in the presence of drug are significantly different than GABA currents alone,
234 (paired t-tests $p<0.0001$).
235
236 We used the same methods to evaluate the effects of purified DBI (50μM) on GABA
237 EC20 currents from $\alpha_3\beta_3\gamma_{2L}$ and $\alpha_5\beta_3\gamma_{2L}$ GABARs. DBI weakly inhibited GABA currents from
238 $\alpha_3\beta_3\gamma_2$ GABARs (Fig. 3). Current amplitudes in the presence of DBI were significantly different
239 from currents elicited by GABA alone (Fig. 3C, paired t-test $p<0.0001$). In contrast, DBI
240 significantly potentiated GABA currents from $\alpha_5\beta_3\gamma_{2L}$ GABARs 1.3-fold (Fig 3, paired t-test

241 $p<0.0001$). The data indicate that DBI acts as a very weak NAM for α3-containing receptors and
242 a PAM for α5-containing receptors (Fig 3).
243 α3 and α5 are homologous GABAR subunit isoforms with many conserved residues
244 (73% identity) [28]. To explore potential mechanisms underlying DBI's actions on α3-containing
245 versus α5-containing GABARs, we constructed $\alpha_3\beta_3\gamma_{2L}$ and $\alpha_5\beta_3\gamma_{2L}$ GABAR homology models
246 and examined protein-protein interactions with DBI using ClusPro, a web-based program for
247 computational docking of proteins [22-24]. This program generates clusters which represent
248 populations of structures where the ligand has docked with low energy at similar locations on
249 the protein. Clusters are ranked based on population size.
250 For both $\alpha_3\beta_3\gamma_{2L}$ and $\alpha_5\beta_3\gamma_{2L}$ GABARs , ClusPro generated many highly populated
251 clusters with DBI bound at the BZD α/γ binding site interface (Fig.4). A flexible loop between the
252 second and third α helices of DBI penetrates under Loop C of the BZD binding site. Residues in
253 this loop code for a DBI proteolytic peptide call octadecaneuropeptide (ODN) that has been
254 shown to displace ^{3}H-BZD binding [29]. We selected two clusters, which showed the closest
255 ODN-BZD site interactions, for further analysis. Fig 4A shows DBI docked at GABAR α_3/γ_{2L} and
256 α_5/γ_{2L} subunit interfaces. Fig 4B highlights differences in residues in the α3 and α5 GABAR
257 subunits, located at the BZD binding site interface, that are within H-bonding distance to DBI.
258 Fig 4C highlights differences in DBI residues that interact with the α3 and α5 GABAR subunits.
259 Residues in the GABAR γ2L subunit interacting with DBI and residues in DBI interacting with
260 the γ2L subunit are displayed in Figs. 4D and E, respectively.
261
262 **Fig 4 – Computational docking reveals DBI can bind at the GABAR α/γ BZD binding site**
263 **interface.** (A) Side views of α_3/γ_{2L} and $\alpha_5\gamma_{2L}$ GABAR subunits (α-yellow, γ-magenta) from
264 homology models based on $\alpha_1\beta_3\gamma_{2L}$ cryoEM model (PDB 6HUO) showing DBI in blue (PDB
265 2FJ9) bound at the BZD α/γ binding site interface with flexible ODN loop under Loop C of the
266 BZD binding site. *In silico* dockings performed using ClusPro as described in Methods. B)

267 Extracellular domains of α3 and α5 GABAR subunits with residues predicted to H-bond to DBI
268 shown in stick and colored red. α3 and α5 GABAR sequence alignments shown below, with H-
269 bonding residues highlighted in red and non-identical residues underlined. C) DBI with residues
270 predicted to H-bond to α_3 and α_5 subunits shown in stick and colored in green. DBI sequences
271 shown below with H-bonding residues colored green. D) Extracellular domain of γ GABAR
272 subunit with residues predicted to H-bond to DBI shown in stick and colored blue. E) DBI with
273 residues predicted to H-bond to γ subunit shown in stick and colored grey. DBI sequences
274 shown below. For the highlighted hydrophobic residues such as DBI G46, M47, and L48, H-
275 bonding is via the backbone, not the residue side-chain.
276
277 When comparing DBI bound to α3 and α5-containing receptors, several differences in
278 interactions between DBI and the GABAR were observed. The GABAR α5 subunit had more
279 residues predicted to H-bond to DBI than the α3 subunit. For example, the α3 histidine at
280 position 142 in Loop7 is not predicted to H-bond with DBI but the aligned α5 glutamine does. In
281 Loop C, the α3 Ile202 does not H-bond with DBI but the aligned α5 asparagine does. In
282 addition, DBI had more H-bond interactions with the γ subunit of α5-containing GABARs.
283 Overall, the computational dockings provide support for the idea that DBI can bind at the BZD
284 binding site interface of GABARs with its flexible ODN loop buried in the BZD binding pocket.
285 The dockings provide a framework for revealing structural mechanisms underlying DBI effects
286 on GABARs.

287 Discussion

288 Despite the fact that DBI was identified as a putative endozepine in the mid-1980s [7],
289 the mechanisms underlying DBI's actions are still unclear. Due to DBI's intracellular roles in
290 long-chain fatty acid metabolism, and its multiple biologically active cleavage products [30-33],
291 direct effects of DBI on GABAR function have not been extensively studied. The use of

292 flumazenil, Ro15-1788 (FLZ, a BZD binding site antagonist) provides indirect evidence for the
293 existence of an endogenous GABAR modulator. Application of this BZD zero-modulator
294 increases the decay of GABA-evoked inhibitory postsynaptic currents in neurons in the
295 hippocampus [34], dentate gyrus [35], neocortex [36] and the thalamic reticular nucleus [8],
296 suggesting that FLZ is displacing an endogenous GABAR modulator. Recording from cells in
297 the thalamic reticular nucleus suggest that DBI positively modulates GABARs [8] while studies
298 in the subventricular zone and hippocampal subgranular cells suggest DBI is a NAM [9, 10]. In
299 this study, using purified DBI and heterologous expression of GABARs, we found that DBI is a
300 PAM for α5-containing GABARs and a weak NAM for α3-containing receptors demonstrating
301 that effects of DBI on GABAR activity are regulated by receptor subunit composition.

302 Recordings from cells in the hippocampal subgranular zone suggest that DBI or its
303 peptide cleavage product, ODN, act as a NAM [10]. Given α5 subunits are highly expressed in
304 the hippocampus [37], we expected that heterologously expressed α5-containing receptors
305 would be negatively modulated by DBI versus positively modulated, which we observed (Fig. 3).
306 Similarly, patch clamp recordings from the thalamic reticular nucleus where α3 is highly
307 expressed [38] suggested that these receptors are positively modulated by DBI [8], while our
308 experiments with heterologously expressed $\alpha_3\beta_3\gamma_{2L}$ GABARs demonstrated that DBI acts as
309 weak NAM (Fig. 3).

310 The differences between data reported here and previously reports are likely due to
311 experimental systems used. In neurons, GABARs are likely associated with accessory subunits
312 such as GARLH or Shisa7 [39, 40], which may alter DBI actions. Furthermore, α3 and α5 are
313 not the only α subunits expressed in the thalamic reticular nucleus and hippocampus,
314 respectively. In native cells, the presence of GABARs comprised of other subunits that may be
315 modulated by DBI make it difficult to assign DBI's effects to one specific GABAR subtype. Here,
316 using a reductionist approach, we demonstrate that DBI is a PAM of $\alpha_5\beta_3\gamma_{2L}$ GABARs and a
317 weak NAM of $\alpha_3\beta_3\gamma_{2L}$ GABARs.

318 $\alpha_5\beta_3\gamma_{2L}$ GABARs are highly expressed in the hippocampus and can be found both
319 synaptically and extrasynaptically[41]. α5-containing GABARs play a large role in hippocampal-
320 dependent forms of learning and memory [42-45]. Our data demonstrating that DBI acts as a
321 PAM for α5-containing receptors suggests that DBI should have effects on learning and
322 memory. Consistent with this idea, DBI-knockout mice display a disruption in spatial learning
323 and memory [46] and social behavior [47]. While somatic IPSP recordings from hippocampal
324 CA1 and dentate gyrus regions found that the DBI knockout did not change the effects of FLZ
325 on mIPSPs [48], these fast IPSPs recorded from the soma of pyramidal neurons are unlikely to
326 capture the effects of DBI on the α5-containing receptors that are expressed primarily in the
327 distal dendritic regions, which are involved in hippocampal learning and memory [49, 50].
328 Dysregulation of GABA-mediated signaling is implicated in a wide variety of neurological
329 diseases and disorders, including Alzheimer's [51, 52], anxiety [4], Parkinson's [53] and epilepsy
330 [2]. Our findings demonstrating that DBI's effects are dependent on GABAR subunit composition
331 lay an important foundation for understanding how inhibition in the brain is regulated.

332 Supporting Information

333 **S1 – Original 15% SDS-PAGE of Fig 1A.** Lanes 1 and 10 show Biorad's Precision Protein
334 Plus All Blue protein standards ranging from 10 kD to 75 kD. Lane 2 shows protein content of
335 the supernatant after emulsion and final high-speed spin. Proteins contained in flow-through,
336 first and second washes are observed in lanes 3, 4 and 5, respectively. Sample was then eluted
337 from the NiNTA column with a single band observed at the expected size of 11kD (lane 6). Lane
338 7 is the flow-through when the sample is loaded onto the PD10 desalting column. Lanes 8 and 9
339 are 6 and 3μL of the PD10 elution, which represents the final, purified and desalted DBI.
340 Overall, we observed the purification of a single ~11 kDa protein, which is the expected size of
341 His-DBI. Boxed area indicates which region of the gel was shown in Fig 1A.

342 **S2 Table – Raw data for GABA dose-response experiments in Fig 2.** Data represent GABA-
343 elicted currents in nA.

344 **S3 Table – Table of data from Fig 3.** Data represent $I_{GABA+Drug}/I_{GABA}$.

345 Acknowledgments

346 We thank the lab of Dr. Henzler-Wildman, University of Wisconsin - Madison for their
347 help with NMR. This study made use of the National Magnetic Resonance Facility at Madison,
348 which is supported by NIH grant P41GM136463, old number P41GM103399 (NIGMS) and
349 P41RR002301. Equipment was purchased with funds from the University of Wisconsin-
350 Madison, the NIH P41GM103399, S10RR02781, S10RR08438, S10RR023438, S10RR025062,
351 S10RR029220), the NSF (DMB-8415048, OIA-9977486, BIR-9214394), and the USDA.
352 Funding for this manuscript from NIH-R21NS099991-01 and NIH-F31NS101804.

353 References:

354 1. Organization WECotSoEDWH. The selection of essential drugs : report of a WHO expert
355 committee [meeting held in Geneva from 17 to 21 October 1977]. Geneva: 1977.

356 2. Palma E, Ruffolo G, Cifelli P, Roseti C, Vliet EAV, Aronica E. Modulation of GABAA
357 Receptors in the Treatment of Epilepsy. Curr Pharm Des. 2017;23(37):5563-8. Epub
358 2017/08/12. doi: 10.2174/1381612823666170809100230. PubMed PMID: 28799512.

359 3. Wisden W, Yu X, Franks NP. GABA Receptors and the Pharmacology of Sleep. Handb
360 Exp Pharmacol. 2019;253:279-304. Epub 2017/10/11. doi: 10.1007/164_2017_56. PubMed
361 PMID: 28993837.

362 4. Engin E, Benham RS, Rudolph U. An Emerging Circuit Pharmacology of GABA A
363 Receptors. Trends in Pharmacological Sciences. 2018;39(8):710-32. doi:
364 10.1016/j.tips.2018.04.003.

365 5. Mohler H. The rise of a new GABA pharmacology. Neuropharmacology. 2011;60(7-
366 8):1042-9. doi: 10.1016/j.neuropharm.2010.10.020. PubMed PMID: ISI:000290648900004.

367 6. Knoflach F, Benke D, Wang Y, Scheurer L, Lüddens H, Hamilton BJ, et al.
368 Pharmacological modulation of the diazepam-insensitive recombinant gamma-aminobutyric
369 acidA receptors alpha 4 beta 2 gamma 2 and alpha 6 beta 2 gamma 2. Mol Pharmacol.
370 1996;50(5):1253-61.

371 7. Guidotti A, Forchetti CM, Corda MG, Konkel D, Bennett CD, Costa E. Isolation,
372 characterization, and purification to homogeneity of an endogenous polypeptide with agonistic
373 action on benzodiazepine receptors. Proc Natl Acad Sci U S A. 1983;80(11):3531-5. Epub
374 1983/06/01. doi: 10.1073/pnas.80.11.3531. PubMed PMID: 6304714; PubMed Central PMCID:
375 PMCPMC394079.

376 8. Christian CA, Herbert AG, Holt RL, Peng K, Sherwood KD, Pangratz-Fuehrer S, et al.
377 Endogenous Positive Allosteric Modulation of GABA(A) Receptors by Diazepam binding
378 inhibitor. Neuron. 2013;78(6):1063-74. doi: 10.1016/j.neuron.2013.04.026. PubMed PMID:
379 ISI:000321026900012.

380 9. Alfonso J, Le Magueresse C, Zuccotti A, Khodosevich K, Monyer H. Diazepam Binding
381 Inhibitor Promotes Progenitor Proliferation in the Postnatal SVZ by Reducing GABA Signaling.
382 Cell Stem Cell. 2012;10(1):76-87. doi: 10.1016/j.stem.2011.11.011. PubMed PMID:
383 ISI:000299449500012.

384 10. Dumitru I, Neitz A, Alfonso J, Monyer H. Diazepam Binding Inhibitor Promotes Stem Cell
385 Expansion Controlling Environment-Dependent Neurogenesis. Neuron. 2017;94(1):125-37.e5.
386 doi: 10.1016/j.neuron.2017.03.003.

387 11. Liu X, Li Y, Zhou L, Chen H, Su Z, Hao W. Conditioned place preference associates with
388 the mRNA expression of diazepam binding inhibitor in brain regions of the addicted rat during
389 withdrawal. 2005;137(1-2):47-54. doi: 10.1016/j.molbrainres.2005.02.021.

390 12. Costa E, Guidotti A. Diazepam Binding Inhibitor (Dbi) - a Peptide with Multiple Biological
391 Actions. Life Sci. 1991;49(5):325-44. doi: Doi 10.1016/0024-3205(91)90440-M. PubMed PMID:
392 ISI:A1991FV18900001.

393 13. Mortensen M, Patel B, Smart TG. GABA potency at GABA(A) receptors found in
394 synaptic and extrasynaptic zones. Front Cell Neurosci. 2012;6. doi: ARTN 1

395 10.3389/fncel.2012.00001. PubMed PMID: ISI:000299807800001.

396 14. Delaglio F, Grzesiek S, Vuister G, Zhu G, Pfeifer J, Bax A. NMRPipe: A multidimensional
397 spectral processing system based on UNIX pipes. J Biomol Nmr. 1995;6(3). doi:
398 10.1007/bf00197809.

399 15. Vranken WF, Boucher W, Stevens TJ, Fogh RH, Pajon A, Llinas M, et al. The CCPN
400 data model for NMR spectroscopy: Development of a software pipeline. Proteins: Structure,
401 Function, and Bioinformatics. 2005;59(4):687-96. doi: https://doi.org/10.1002/prot.20449.

402 16. Venkatachalan SP, Bushman JD, Mercado JL, Sancar F, Christopherson KR, Boileau
403 AJ. Optimized expression vector for ion channel studies in Xenopus oocytes and mammalian
404 cells using alfalfa mosaic virus. Pflugers Arch. 2007;454(1):155-63. Epub 2006/12/05. doi:
405 10.1007/s00424-006-0183-1. PubMed PMID: 17146677.

406 17. Boileau AJ, Kucken AM, Evers AR, Czajkowski C. Molecular dissection of
407 benzodiazepine binding and allosteric coupling using chimeric gamma-aminobutyric acidA
408 receptor subunits. Mol Pharmacol. 1998;53(2):295-303. Epub 1998/03/14. doi:
409 10.1124/mol.53.2.295. PubMed PMID: 9463488.

410 18. Boileau AJ, Baur R, Sharkey LM, Sigel E, Czajkowski C. The relative amount of cRNA
411 coding for gamma2 subunits affects stimulation by benzodiazepines in GABA(A) receptors
412 expressed in Xenopus oocytes. Neuropharmacology. 2002;43(4):695-700. Epub 2002/10/09.
413 doi: 10.1016/s0028-3908(02)00036-9. PubMed PMID: 12367615.

414 19. Hanson SM, Czajkowski C. Structural mechanisms underlying benzodiazepine
415 modulation of the GABA(A) receptor. J Neurosci. 2008;28(13):3490-9. Epub 2008/03/28. doi:
416 10.1523/jneurosci.5727-07.2008. PubMed PMID: 18367615; PubMed Central PMCID:
417 PMCPMC2410040.

418 20. Masiulis S, Desai R, Uchański T, Serna Martin I, Laverty D, Karia D, et al. GABAA
419 receptor signalling mechanisms revealed by structural pharmacology. Nature.
420 2019;565(7740):454-9. doi: 10.1038/s41586-018-0832-5.

421 21. Taskinen JP, Van Aalten DM, Knudsen J, Wierenga RK. High resolution crystal
422 structures of unliganded and liganded human liver ACBP reveal a new mode of binding for the
423 acyl-CoA ligand. 2006;66(1):229-38. doi: 10.1002/prot.21124.

424 22. Kozakov D, Beglov D, Bohnuud T, Mottarella SE, Xia B, Hall DR, et al. How good is
425 automated protein docking? 2013;81(12):2159-66. doi: 10.1002/prot.24403.

426 23. Kozakov D, Hall DR, Xia B, Porter KA, Padhorny D, Yueh C, et al. The ClusPro web
427 server for protein–protein docking. Nature Protocols. 2017;12(2):255-78. doi:
428 10.1038/nprot.2016.169.

429 24. Vajda S, Yueh C, Beglov D, Bohnuud T, Mottarella SE, Xia B, et al. New additions to the
430 ClusPro server motivated by CAPRI. Proteins: Structure, Function, and Bioinformatics.
431 2017;85(3):435-44. doi: 10.1002/prot.25219.

432 25. Shilling PJ, Mirzadeh K, Cumming AJ, Widesheim M, Köck Z, Daley DO. Improved
433 designs for pET expression plasmids increase protein production yield in Escherichia coli.
434 Communications Biology. 2020;3(1). doi: 10.1038/s42003-020-0939-8.

435 26. Karim N, Wellendorph P, Absalom N, Johnston GA, Hanrahan JR, Chebib M. Potency of
436 GABA at human recombinant GABA(A) receptors expressed in Xenopus oocytes: a mini review.
437 Amino Acids. 2013;44(4):1139-49. Epub 2013/02/07. doi: 10.1007/s00726-012-1456-y. PubMed
438 PMID: 23385381.

439 27. Nimmich ML, Heidelberg LS, Fisher JL. RNA editing of the GABA(A) receptor alpha3
440 subunit alters the functional properties of recombinant receptors. Neurosci Res. 2009;63(4):288-
441 93. doi: 10.1016/j.neures.2009.01.003. PubMed PMID: 19367790.

442 28. Duvaud S, Gabella C, Lisacek F, Stockinger H, Ioannidis V, Durinx C. Expasy, the Swiss
443 Bioinformatics Resource Portal, as designed by its users. Nucleic Acids Research.
444 2021;49(W1):W216-W27. doi: 10.1093/nar/gkab225.

445 29. Ferrero P, Santi MR, Conti-Tronconi B, Costa E, Guidotti A. Study of an
446 octadecaneuropeptide derived from diazepam binding inhibitor (DBI): biological activity and
447 presence in rat brain. Proc Natl Acad Sci U S A. 1986;83(3):827-31. Epub 1986/02/01. doi:
448 10.1073/pnas.83.3.827. PubMed PMID: 3456171; PubMed Central PMCID: PMCPMC322958.

449 30. Knudsen J. Acyl-Coa-Binding and Transport, an Alternate Function for Diazepam
450 Binding Inhibitor (Dbi), Which is Identical with Acyl-Coa-Binding Protein. Neuropharmacology.
451 1991;30:1405-10.

452 31. Bouyakdan K, Taib B, Budry L, Zhao SG, Rodaros D, Neess D, et al. A novel role for
453 central ACBP/DBI as a regulator of long-chain fatty acid metabolism in astrocytes. J
454 Neurochem. 2015;133(2):253-65. doi: 10.1111/jnc.13035. PubMed PMID:
455 ISI:000352796000010.

456 32. Slobodyansky E, Guidotti A, Wambebe C, Berkovich A, Costa E. Isolation and
457 characterization of a rat brain triakontatetraneuropeptide, a posttranslational product of
458 diazepam binding inhibitor: specific action at the Ro 5-4864 recognition site. J Neurochem.
459 1989;53(4):1276-84. Epub 1989/10/01. doi: 10.1111/j.1471-4159.1989.tb07425.x. PubMed
460 PMID: 2769267.

461 33. Tonon MC, Vaudry H, Chuquet J, Guillebaud F, Fan J, Masmoudi-Kouki O, et al.
462 Endozepines and their receptors: Structure, functions and pathophysiological significance.
463 Pharmacol Ther. 2020;208:107386. Epub 2019/07/10. doi: 10.1016/j.pharmthera.2019.06.008.
464 PubMed PMID: 31283949.

465 34. King GL, Knox JJ, Dingledine R. Reduction of inhibition by a benzodiazepine antagonist,
466 Ro15-1788, in the rat hippocampal slice. 1985;15(2):371-8. doi: 10.1016/0306-4522(85)90219-
467 2.

468 35. Leroy C, Poisbeau P, Keller AF, Nehlig A. Pharmacological plasticity of GABA A
469 receptors at dentate gyrus synapses in a rat model of temporal lobe epilepsy. 2004;557(2):473-
470 87. doi: 10.1113/jphysiol.2003.059246.

471 36. Ali AB, Thomson AM. Synaptic 5 Subunit-Containing GABAA Receptors Mediate IPSPs
472 Elicited by Dendrite-Preferring Cells in Rat Neocortex. Cerebral Cortex. 2008;18(6):1260-71.
473 doi: 10.1093/cercor/bhm160.

474 37. Sequeira A, Shen K, Gottlieb A, Limon A. Human brain transcriptome analysis finds
475 region- and subject-specific expression signatures of GABAAR subunits. Communications
476 Biology. 2019;2(1). doi: 10.1038/s42003-019-0413-7.

477 38. Hörtnagl H, Tasan RO, Wieselthaler A, Kirchmair E, Sieghart W, Sperk G. Patterns of
478 mRNA and protein expression for 12 GABAA receptor subunits in the mouse brain.
479 Neuroscience. 2013;236:345-72. Epub 2013/01/23. doi: 10.1016/j.neuroscience.2013.01.008.
480 PubMed PMID: 23337532; PubMed Central PMCID: PMCPMC3605588.

481 39. Yamasaki T, Hoyos-Ramirez E, Martenson JS, Morimoto-Tomita M, Tomita S. GARLH
482 Family Proteins Stabilize GABA(A) Receptors at Synapses. Neuron. 2017;93(5):1138-52.e6.
483 doi: 10.1016/j.neuron.2017.02.023. PubMed PMID: 28279354.

484 40. Han W, Li J, Pelkey KA, Pandey S, Chen X, Wang Y-X, et al. Shisa7 is a
485 GABA_A receptor auxiliary subunit controlling benzodiazepine actions. Science.
486 2019;366(6462):246-50. doi: 10.1126/science.aax5719.

487 41. Mortensen M, Patel B, Smart TG. GABA Potency at GABAA Receptors Found in
488 Synaptic and Extrasynaptic Zones. Front Cell Neurosci. 2012;6. doi: 10.3389/fncel.2012.00001.

42. Collinson N, Atack JR, Laughton P, Dawson GR, Stephens DN. An inverse agonist selective for alpha5 subunit-containing GABAA receptors improves encoding and recall but not consolidation in the Morris water maze. Psychopharmacology (Berl). 2006;188(4):619-28. Epub 2006/04/25. doi: 10.1007/s00213-006-0361-z. PubMed PMID: 16633803.

43. Joksimović S, Divljaković J, Van Linn ML, Varagic Z, Brajković G, Milinković MM, et al. Benzodiazepine-induced spatial learning deficits in rats are regulated by the degree of modulation of α1 GABAA receptors. European Neuropsychopharmacology. 2013;23(5):390-9. doi: https://doi.org/10.1016/j.euroneuro.2012.05.003.

44. Timić T, Joksimović S, Milić M, Divljaković J, Batinić B, Savić MM. Midazolam impairs acquisition and retrieval, but not consolidation of reference memory in the Morris water maze. Behavioural Brain Research. 2013;241:198-205. doi: https://doi.org/10.1016/j.bbr.2012.12.014.

45. Crestani F, Keist R, Fritschy J-M, Benke D, Vogt K, Prut L, et al. Trace fear conditioning involves hippocampal α₅ GABA_A receptors. Proceedings of the National Academy of Sciences. 2002;99(13):8980-5. doi: 10.1073/pnas.142288699.

46. Ujjainwala AL, Courtney CD, Wojnowski NM, Rhodes JS, Christian CA. Differential impacts on multiple forms of spatial and contextual memory in diazepam binding inhibitor knockout mice. Journal of Neuroscience Research. 2019. doi: 10.1002/jnr.24393.

47. Ujjainwala AL, Courtney CD, Rhoads SG, Rhodes JS, Christian CA. Genetic loss of diazepam binding inhibitor in mice impairs social interest. Genes, Brain and Behavior. 2018;17(5):e12442. doi: 10.1111/gbb.12442.

48. Courtney CD, Christian CA. Subregion-Specific Impacts of Genetic Loss of Diazepam Binding Inhibitor on Synaptic Inhibition in the Murine Hippocampus. Neuroscience. 2018;388:128-38. doi: 10.1016/j.neuroscience.2018.07.012.

49. Rodgers FC, Zarnowska ED, Laha KT, Engin E, Zeller A, Keist R, et al. Etomidate Impairs Long-Term Potentiation In Vitro by Targeting 5-Subunit Containing GABAA Receptors on Nonpyramidal Cells. J Neurosci. 2015;35(26):9707-16. doi: 10.1523/jneurosci.0315-15.2015.

50. Groen MR, Paulsen O, Pérez-Garci E, Nevian T, Wortel J, Dekker MP, et al. Development of dendritic tonic GABAergic inhibition regulates excitability and plasticity in CA1 pyramidal neurons. Journal of Neurophysiology. 2014;112(2):287-99. doi: 10.1152/jn.00066.2014. PubMed PMID: 24760781.

51. Calvo-Flores Guzmán B, Vinnakota C, Govindpani K, Waldvogel HJ, Faull RLM, Kwakowsky A. The GABAergic system as a therapeutic target for Alzheimer's disease. J Neurochem. 2018;146(6):649-69. doi: 10.1111/jnc.14345.

52. Govindpani K, Calvo-Flores Guzmán B, Vinnakota C, Waldvogel HJ, Faull RL, Kwakowsky A. Towards a Better Understanding of GABAergic Remodeling in Alzheimer’s Disease. International Journal of Molecular Sciences. 2017;18(8):1813. PubMed PMID: doi:10.3390/ijms18081813.

53. Brickley SG, Mody I. Extrasynaptic GABA(A) receptors: their function in the CNS and implications for disease. Neuron. 2012;73(1):23-34. doi: 10.1016/j.neuron.2011.12.012. PubMed PMID: 22243744.

529

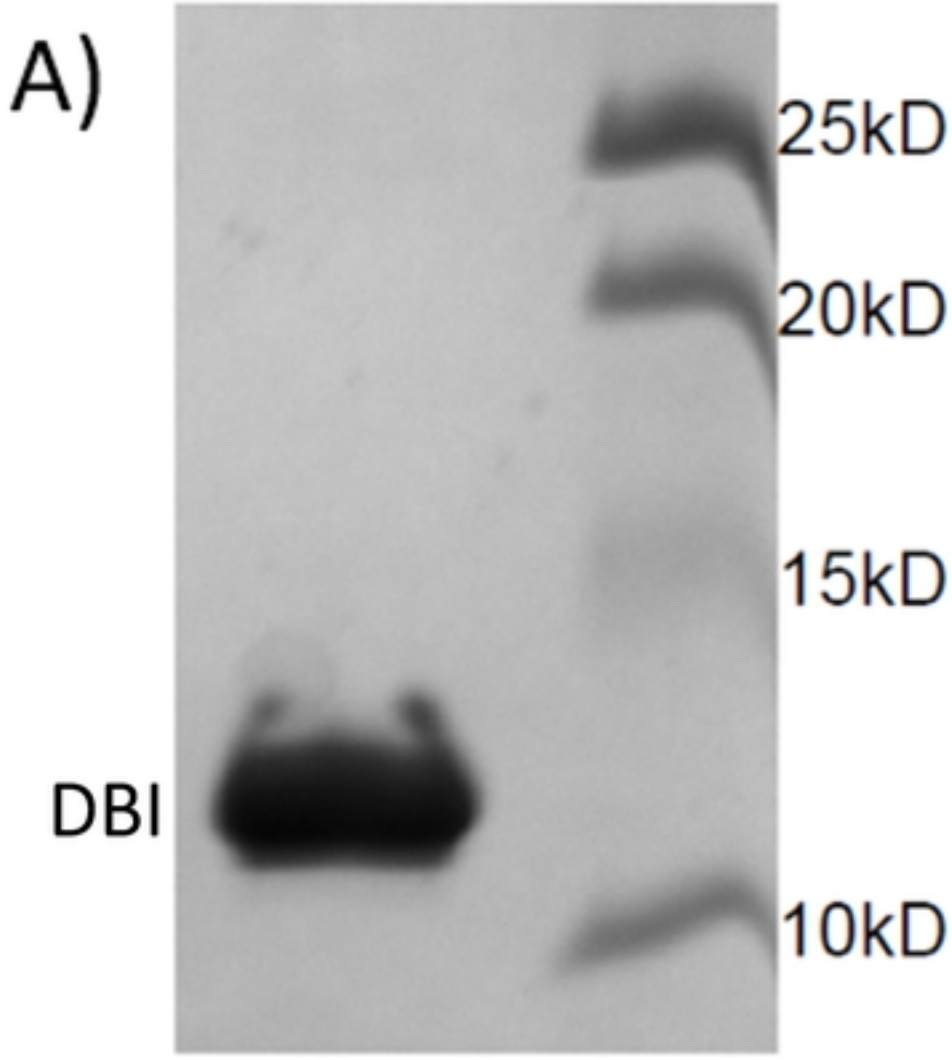
A)
25kD
20kD
15kD
DBI
10kD

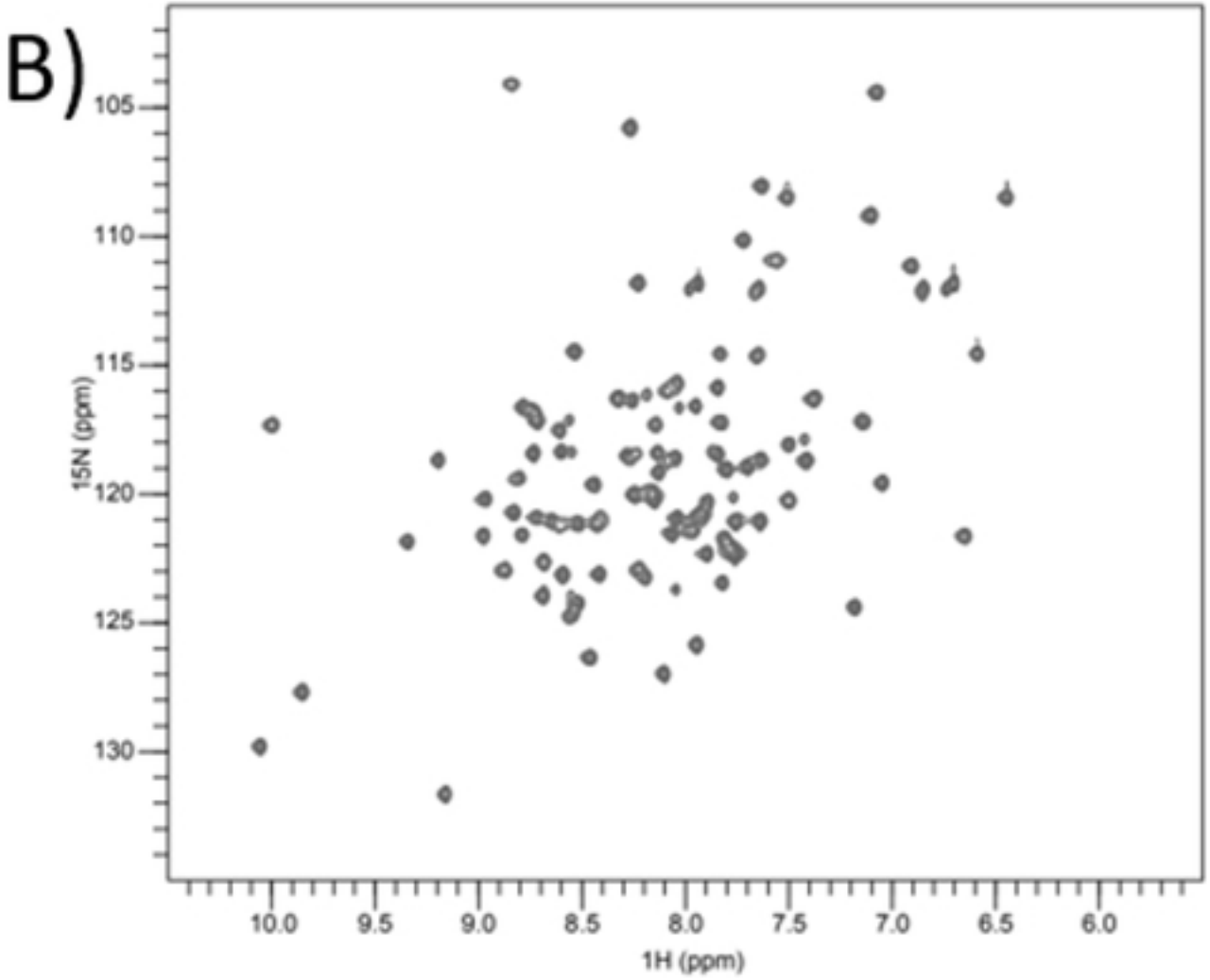
B)
105
110
115
120
125
130
15N (ppm)
10.0
9.5
9.0
8.5
8.0
7.5
7.0
6.5
6.0
1H (ppm)

Figure

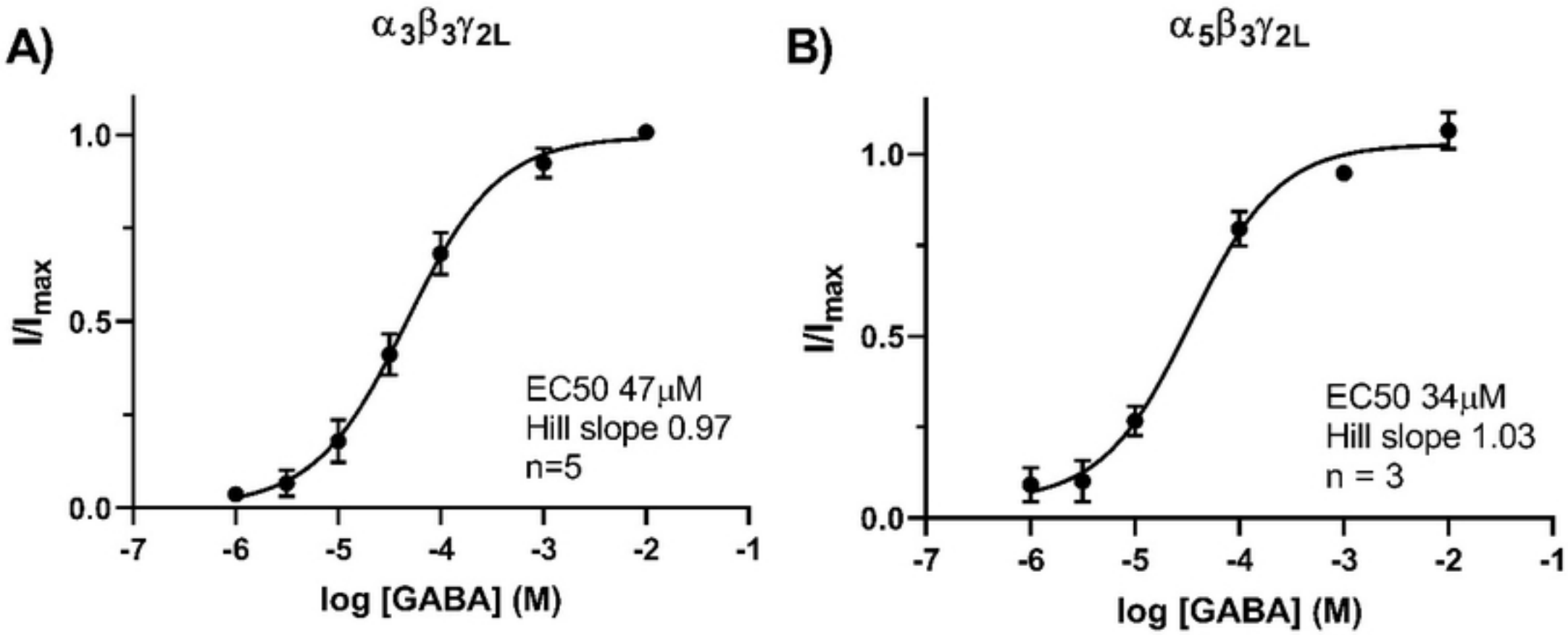
A)
$\alpha_3\beta_3\gamma_{2L}$
1.0
0.5
0.0
I/I_{max}
EC50 47μM
Hill slope 0.97
n=5
-7
-6
-5
-4
-3
-2
-1
log [GABA] (M)
B)
$\alpha_5\beta_3\gamma_{2L}$
1.0
0.5
0.0
I/I_{max}
EC50 34μM
Hill slope 1.03
n = 3
-7
-6
-5
-4
-3
-2
-1
log [GABA] (M)

Figure

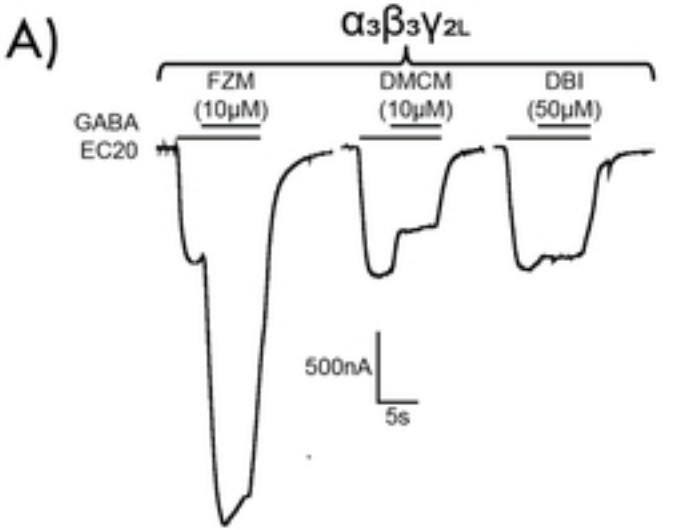

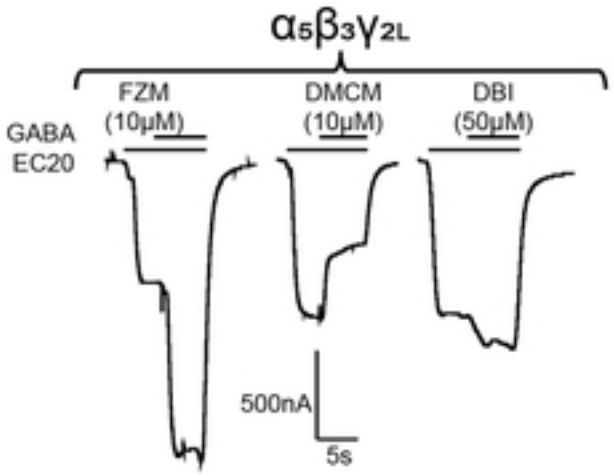

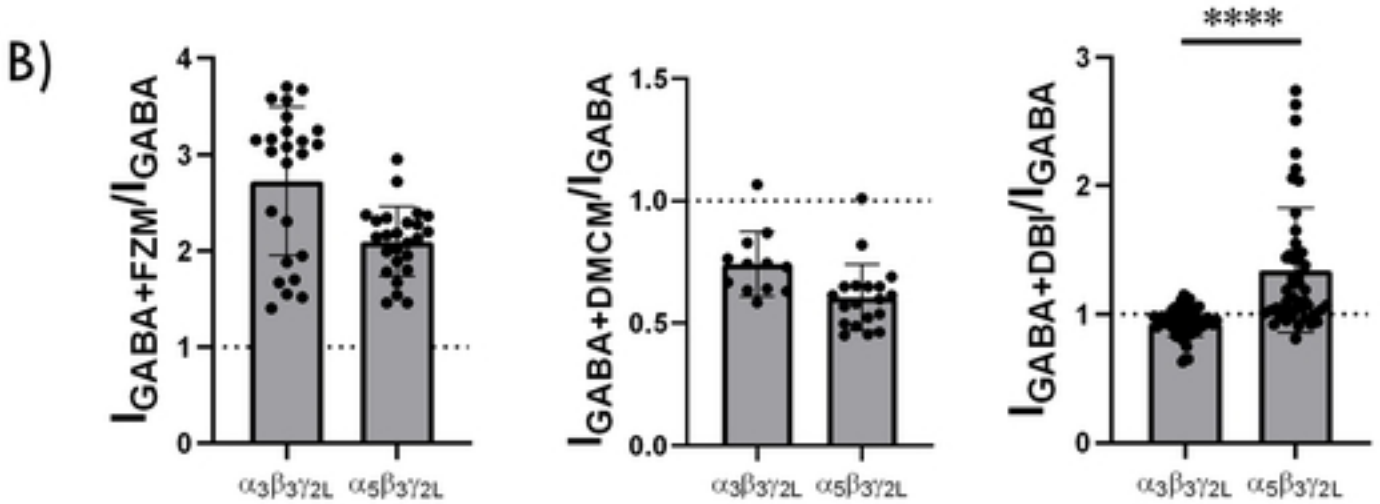

C)

	$\alpha_3\beta_3\gamma_{2L}$			$\alpha_5\beta_3\gamma_{2L}$		
	FZM	DMCM	DBI	FZM	DMCM	DBI
Mean	2.72±0.77	0.74±0.13	0.93±0.11	2.10±0.36	0.61±0.14	1.34±0.48
n	24	12	54	25	19	47
p-Value	<0.0001	<0.0001	<0.0001	<0.0001	<0.0001	<0.0001

Figure

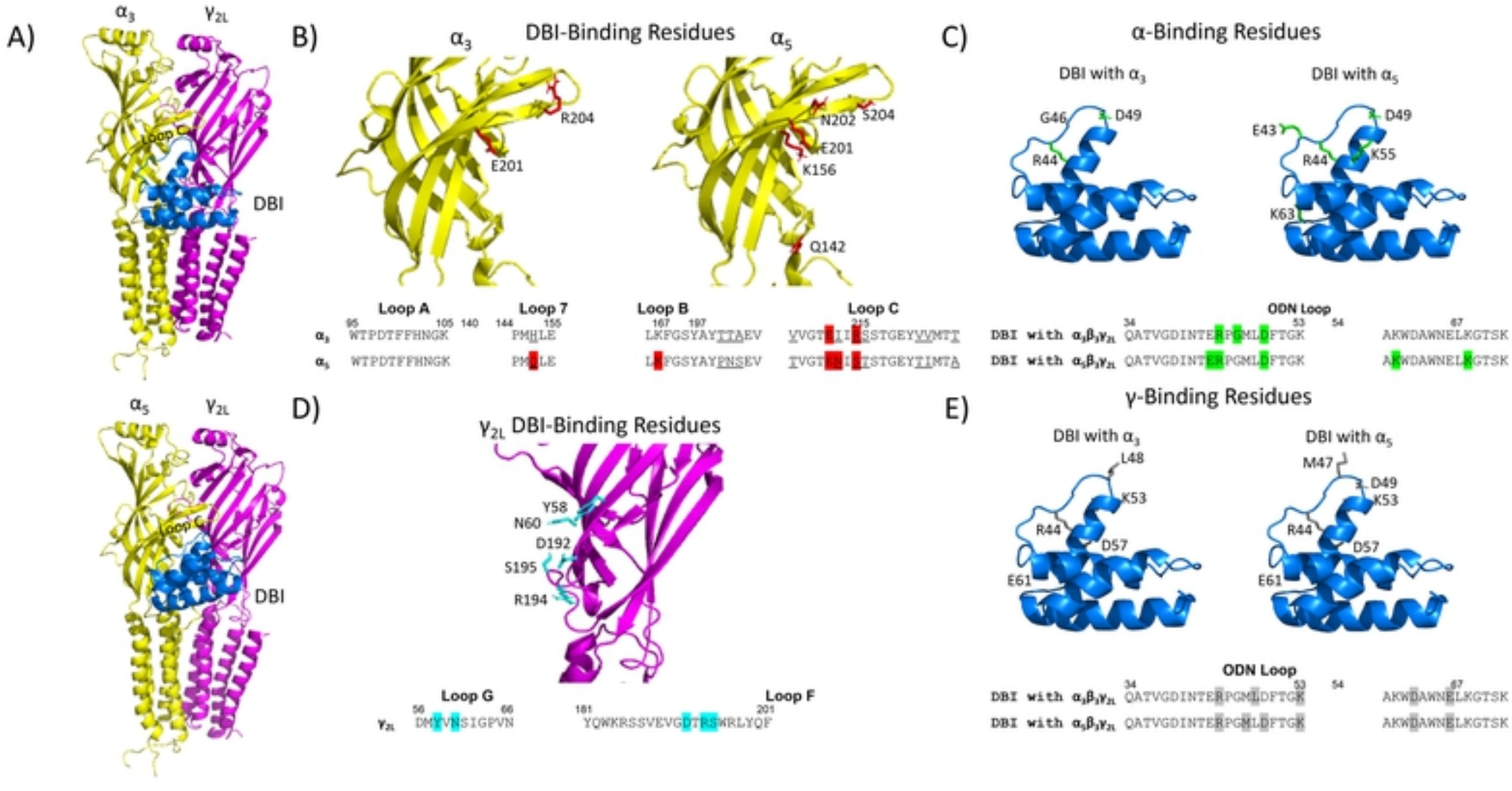
A)
α3
γ2L
Loop C
DBI
B)
DBI-Binding Residues
α3
R204
E201
α5
N202
S204
E201
K156
Q142
Loop A
Loop 7
Loop B
Loop C
C)
α-Binding Residues
DBI with α3
G46
D49
R44
DBI with α5
E43
D49
R44
K55
K63
ODN Loop
α5
γ2L
Loop C
DBI
D)
γ2L DBI-Binding Residues
Y58
N60
D192
S195
R194
Loop G
Loop F
E)
γ-Binding Residues
DBI with α3
L48
K53
R44
D57
E61
DBI with α5
M47
D49
K53
R44
D57
E61
ODN Loop

Figure